Nijmegen Preprint
HEN-346
September 1991

Large Scale Application of Magnetoresistors in the Magnetic Field Measuring System of the L3 Detector

C. Brouwer, F.J.G.H. Crijns, A.C. König, J.M. Lubbers*, C.L.A. Pols, D.J. Schotanus
University of Nijmegen and NIKHEF-H, Nijmegen, The Netherlands

K. Freudenreich
Eidgenössische Technische Hochschule, ETH, Zürich, Switzerland

J. Onvlee**
National Institute for High Energy Physics, NIKHEF, Amsterdam, The Netherlands

D. Luckey
Massachusetts Institute of Technology, Cambridge, United States of America

F. Wittgenstein
European Laboratory for Particle Physics, CERN, Geneva, Switzerland

Abstract

The design and implementation of the magnetic field measuring system of the L3 detector is described. The system features 992 permanently installed magnetoresistors which serve the mapping of the nominally 0.5 Tesla field of the L3 magnet over its entire 1200 m^3 volume. It enables the reconstruction of the magnetic field to an accuracy of better than 0.4 %. To allow the magnetoresistors to be used over an extended range of ambient temperatures, a passive temperature compensation scheme has been devised. An internally calibrated read-out system under micro-processor control facilitates easy access to the magnetic field data. Furthermore, the mechanical design of the system, its calibration and the field reconstruction procedures are described.

Submitted to Nuclear Instruments and Methods in Physics Research A.

* Now at CERN, Geneva, Switzerland
** Now at Océ Nederland bv, Venlo, The Netherlands

Nijmegen Preprint
HEN-346
September 1991

Large Scale Application of Magnetoresistors in the Magnetic Field Measuring System of the L3 Detector

C. Brouwer, F.J.G.H. Crijns, A.C. König, J.M. Lubbers*, C.L.A. Pols, D.J. Schotanus
University of Nijmegen and NIKHEF-H, Nijmegen, The Netherlands

K. Freudenreich
Eidgenössische Technische Hochschule, ETH, Zürich, Switzerland

J. Onvlee**
National Institute for High Energy Physics, NIKHEF, Amsterdam, The Netherlands

D. Luckey
Massachusetts Institute of Technology, Cambridge, United States of America

F. Wittgenstein
European Laboratory for Particle Physics, CERN, Geneva, Switzerland

Abstract

The design and implementation of the magnetic field measuring system of the L3 detector is described. The system features 992 permanently installed magnetoresistors which serve the mapping of the nominally 0.5 Tesla field of the L3 magnet over its entire 1200 m^3 volume. It enables the reconstruction of the magnetic field to an accuracy of better than 0.4 %. To allow the magnetoresistors to be used over an extended range of ambient temperatures, a passive temperature compensation scheme has been devised. An internally calibrated read-out system under micro-processor control facilitates easy access to the magnetic field data. Furthermore, the mechanical design of the system, its calibration and the field reconstruction procedures are described.

Submitted to Nuclear Instruments and Methods in Physics Research A.

---

* Now at CERN, Geneva, Switzerland
** Now at Océ Nederland bv, Venlo, The Netherlands

1. Introduction

The L3 detector is the largest of the four detectors presently operating at the LEP e^+e^- collider at CERN. It focusses on high resolution energy measurements of electrons, photons, and muons. The active detector components are installed inside a very large, solenoidal magnet and arranged coaxially around the beam pipe. From the interaction point outwards one encounters a charged particle tracking device (TEC), a BGO high resolution electromagnetic calorimeter, a uranium hadron calorimeter, and a muon spectrometer. The axial magnetic field of 0.5 T (5 kG) enables the determination of the charged particle momenta in the central tracking chamber and in the muon detector. A general view of the L3 detector is presented in fig. 1. A detailed description of the entire detector and its components is given in ref. [1].

The muon spectrometer is designed to give a momentum resolution of $\Delta p/p \leq 2\,\%$ at $p = 50\,\mathrm{GeV/c}$. It consists of three concentric layers of drift chambers (fig. 2) which measure the sagitta s of the muon tracks (fig. 3). From the sagitta measurement, the tranverse component p_t of the muon momentum can be calculated by means of the relation

$$p_t = \frac{0.2998 \cdot B_z \cdot L^2}{8 \cdot s}.$$

Here B_z is the main (axial) component of the magnetic field and L is the projection of the track length in the muon spectrometer onto a plane perpendicular to B_z. Note that for a given accuracy of the sagitta measurement, the momentum resolution $\Delta p_t/p_t$ varies linearly with B_z and quadratically with the track length L. For this reason the L3 collaboration has opted for a moderate magnetic field ($B_z \simeq 0.5\,\mathrm{T}$) over a large track length ($L \simeq 2.9\,\mathrm{m}$). In this configuration a 45 GeV/c muon from Z^0 decay gives a sagitta of 3.7 mm. A large volume magnet has been built consisting of an octagonal aluminium coil surrounded by a soft iron return yoke. The magnet has an inner diameter of 11.4 m, an inner length of 11.9 m, and a total weight of 7800 t. For a 0.5 T field, it uses 4.2 MW of electrical power

In order to meet the design resolution on the muon momentum of $\Delta p_t/p_t \leq 2\,\%$, both the sagitta s and the magnetic field B_z must be known to sufficient accuracy. The accuracy of the field enters twice into the calculation of the muon momentum: once via the relation between the sagitta s and p_t, and once through the relation between drift time and drift distance. A detailed error propagation analysis yields the following requirements on ΔB inside the drift chambers: $\Delta B_z \leq 2 \cdot 10^{-3}\,\mathrm{T}$ and $\Delta B_r \leq 20 \cdot 10^{-3}\,\mathrm{T}$ [2]. For the main field component B_z of 0.5 T, this implies a relative accuracy of $\Delta B_z/B_z \leq 0.4\,\%$.

Because of the large volume, which is furthermore obstructed by the support tube (see fig. 1), the field measurement has been divided into two parts: The inner volume of the support tube was mapped with Hall plates prior to the installation of detector components. In addition, a series of NMR readings has been taken along the central axis of the detector. Outside the support tube, only a limited number of such field measurements have been made, namely on the inner surface of one of

the magnet poles. The remaining volume, which houses the muon spectrometer, is mapped by means of a permanently installed field measuring system consisting of about one thousand field sensors attached directly to the muon drift chambers. In addition five permanently installed NMR probes monitor the absolute value of the field.

In this paper we describe the field measuring system and its application. We commence in section 2 with a discussion of a 2-dimensional (2-D) field calculation, the results of which have guided the design of the system. In section 3 we investigate the properties of the magnetoresistor devices which are being used as field sensors. The next section describes the electronical and mechanical design of the system. In section 5 various approaches to reconstruction of the field from the measured values are discussed. Section 6 gives a summary and conclusions.

2. Field Calculations

To estimate the strength and shape of the L3 magnetic field, a 2-D model approach has been adopted [3]. In this model, the octagonal symmetry of the L3 magnet is approximated by a rotational one, thus reducing the relevant field components to B_z and B_r, and ignoring B_φ. All radii in the model are chosen equal to the average radii of the corresponding octagonal structures, which is 2.7 % larger than the radius of the inscribed circle of the octagon (or, equivalently, 5.4 % smaller than that of its circumscribed circle). Accordingly, the return yoke is modeled as an iron cylinder of 0.8 m thickness with end poles of 1 m thick. The end poles have a circular hole in the middle and a 0.1 m wide circular slit to account for the rabbets of the moveable iron doors. The coil is modeled as a single turn with a thickness and total width equal to that of the real coil and a homogeneous current density corresponding to the real number of Ampère-turns.

The field components B_z and B_r have been calculated by means of the computer code POISSON [4]. The field at the muon drift chamber positions is obtained by evaluating the 2-D model at the actual r-values of the drift chambers. The resulting B_z-values along the centre and along the edge of the outer surface of an octant are presented graphically in fig. 4. For the fiducial volume of the detector, the most important quantitative results of the field calculations are that the main field component B_z lies in the range of 0.45 to 0.53 T, that its derivative $dB_z/dz \leq 0.2\,\mathrm{T/m}$, and that the radial field component $B_r \leq 0.09\,\mathrm{T}$.

Field calculations have also been performed using the 3-D program TOSCA [5], adopting a simpler model of the magnet which ignores the rabbet slits. Comparison of the TOSCA results with a POISSON calculation for this same model, shows only small differences close to the central holes in the pole pieces.

3. Field Sensors

In this section we discuss the properties of the magnetoresistor devices which are used as sensors in the field measuring system. Since the system had to fit in the existing designs of the magnet and the muon chambers, it had to be squeezed into the few centimeters of space between the outer surface of the muon detector and the heat shield inside the magnet coil. Important additional design considerations were the total number of probes and their positions. Since the total surface of the muon chambers is about $1000\,\mathrm{m}^2$, a straightforward uniform sampling of the field over the entire surface would easily result in several thousands of probes. It was therefore decided to sample more often in regions where the field has large variations and less often in those regions where the field is more uniform. Nevertheless, the number of installed sensors is about one thousand. These considerations implied the following selection criteria for field sensors:

- The sensors had to be small, since the system had to fit in a space of typically a few cm's high,
- The sensors needed to be relatively inexpensive, given the large number required,
- The sensors of course needed to be sufficiently accurate and stable.

3.1 Magnetoresistors

In view of these requirements, Siemens magnetoresistors of the type FP30N60 K (the suffix K indicating a ceramic backing) are selected. These devices have a field dependent resistance. They are indeed small (some $1 \times 3\,\mathrm{mm}^2$) and also inexpensive ($\sim$ SFr. 10). For our application, these magnetoresistors have a number of advantages over equally inexpensive Hall plates: As the magnetoresistors are insensitive to the sign of B, they are both easier to calibrate and less sensitive to angular alignment errors (cf. section 3.3). In addition, they have only two (rather than four) terminal leads. A feasibility study, the results of which are described below, has established the utility of the magnetoresistors.

Magnetoresistors are semiconductor devices based on the Hall effect. They are made of $InSb$ interspersed with thin, parallel needles of $NiSb$ [6]. Applying a voltage over a slab of this material will cause an electric current to flow which, in the absence of a magnetic field, will experience a resistance R_0 (fig. 5a). A magnetic field B normal to the magnetoresistor would change the direction of the current by some angle. In the absence of the $NiSb$ needles, a Hall voltage would develop across the slab which would straighten out the current flow. The needles, however, have a very low resistivity and in a sense internally "short-circuit" the Hall voltage. The overall effect is that the current follows some zig-zag path through the slab (fig. 5b), the result being an increased resistance. For moderate magnetic fields ($B \leq 0.3\,\mathrm{T}$) the resulting resistance R_B has a nearly quadratic B-dependence. For higher fields this dependence gradually becomes linear.

Fig. 6 shows the measured R_B behaviour of three FP30N60 K magnetoresistors. Typically $R_0 = 60\,\Omega \pm 20\,\%$ while the $R_{0.5}$-values lie in the 160 to 220 Ω range. From the curves one sees that at 0.5 T the B-dependence indeed is almost linear with a slope $\frac{dR}{dB}\big|_{0.5}$ of about 350 Ω/T.

3.2 Temperature Compensation

Unfortunately, the magnetoresistance R_{MR} shows a large, negative, temperature coefficient which, to make things worse, is even field dependent. In a 0.5 T field its value σ_{MR} is typically of the order $-0.17\,\%$/K (see fig. 7a). Given the fact that the ambient temperature in the experimental hall has variations of plus or minus a few degrees, this effect is incompatible with the required accuracy of 0.4 %. The solution is to compensate the thermal variation of the magnetoresistance by placing a (field independent) positive temperature coefficient resistor (PTC) in parallel. For a given R_{PTC} and temperature coefficient σ_{PTC}, the condition for cancellation of temperature effects is

$$\frac{\sigma_{PTC}}{R_{PTC}} + \frac{\sigma_{MR}}{R_{MR}} = 0.$$

Having at our disposal PTC's with $\sigma_{PTC} = +0.35\,\%/^oC$, the required value of R_{PTC} can be calculated once R_{MR} and σ_{MR} are known. Fig. 7b shows that this temperature compensation scheme reduces the net temperature drift to less than 0.10 % over the temperature range from 16 °C to 28 °C. As both R_{MR} and σ_{MR} show a large variation, application of the compensation scheme requires that both quantities be determined for each magnetoresistor individually. The two parameters also depend on the magnetic field strength, so these measurements have to be done in a 0.5 T field. Although cancellation of temperature effects is only exact for this particular field strength, measurements show that the compensation is still sufficiently effective in a 0.4 T field (see fig. 7c).

A slight drawback of the temperature compensation scheme is that the absolute sensitivity becomes smaller. Using the R-values at 0.4 and 0.5 T from figs. 7b and 7c, we estimate the slope $\frac{dR}{dB}\big|_{0.5}$ for a compensated magnetoresistor to be $\simeq 170\,\Omega$/T (at $R_{0.5} \simeq 115\,\Omega$).

3.3 Minor Field Components

Before adopting the magnetoresistors to measure the main component B_z of the L3 magnetic field, we verify that this measurement is not spoiled by the minor field component B_r. To that end, we test a calibrated magnetoresistor in a homogeneous field B of 0.5 T under various angles θ with respect to the field. In this way the probe is simultaneously exposed to a normal component $B_n = B\cos\theta$ and a surface component $B_s = B\sin\theta$. The resistance as a function of θ is measured and, by means of the known calibration, converted to "effective" field values $\widetilde{B}(\theta)$. We find $\widetilde{B}(\theta)$ to

obey the following empirical relation:

$$\widetilde{B}(\theta) = B \cdot \sqrt{\cos^2\theta + \alpha^2 \sin^2\theta} = \sqrt{B_n^2 + \alpha^2 B_s^2}\,.$$

Obviously, the coefficient α must be interpreted as the fraction of the surface component B_s "sensed" by the magnetoresistor. We determine the coefficient α for rotations around each of the two axes I and II indicated in fig. 8, the result being $\alpha_I^2 \simeq 0.04$ and $\alpha_{II}^2 \simeq 0.01$. It should be mentioned here that the above empirical relation is only observed for magnetoresistors on a ceramic substrate (type FP30N60 K). The same devices on an insulated iron substrate (type FP30N60 E) show a completely different behaviour.

The finite values of the coefficients α imply that a measurement of the component B_z by means of a magnetoresistor facing the z-direction, is affected by the presence of the non-zero B_r component. Taking the outer surface of an octant as a reference plane, B_r gives rise to a "horizontal" and a "vertical" field component B_h and B_v in the plane of the magnetoresistor (see fig. 9). Due to these non-vanishing components, a measurement of B_z will yield the effective field $\widetilde{B}$:

$$\widetilde{B} = \sqrt{B_z^2 + \alpha_I^2 B_h^2 + \alpha_{II}^2 B_v^2} = B_z \cdot \sqrt{1 + \alpha_I^2 (B_h/B_z)^2 + \alpha_{II}^2 (B_v/B_z)^2}.$$

The difference of B_z and $\widetilde{B}$ is a contribution to the measurement error ΔB_z. To estimate this contribution, we observe that $B_v = B_r \cdot \cos\varphi$ and $B_h = B_r \cdot \sin\varphi$ (fig. 9). For a constant B_r, the maximum values for B_v and B_h are found for $\varphi = 0^o$ ($B_v = B_r$) and $\varphi = 22.5^o$ ($B_h \simeq 0.38 \cdot B_r$) respectively. From the field calculations (cf. section 2) $B_r \leq 0.09\,\mathrm{T}$ and $0.45\,\mathrm{T} \leq B_z \leq 0.53\,\mathrm{T}$, hence $B_v/B_z \leq 0.20$ and $B_h/B_z \leq 0.08$ over the entire volume of the detector. Inserting these limits and the numerical values of the coefficients α, we find a worst case error contribution of $\Delta B_z/B_z \simeq 0.03\,\%$.

Similar considerations show that an anticipated angular misalignment of some 2.5^o ($\simeq 45\,\mathrm{mrad}$) gives rise to another error contribution $\Delta B_z/B_z \simeq 0.10\,\%$.

Analogously to the effect of angular misalignment, we have to consider the effect of a longitudinal position error Δz, which introduces a measurement uncertainty $\Delta B = (dB_z/dz)\Delta z$. For an estimated Δz of less than 2 cm, and using $dB_z/dz \leq 0.2\,\mathrm{T/m}$ from the field calculations (cf. section 2), we find $\Delta B_z/B_z \leq 0.08\,\%$.

In conclusion we expect the following worst case contributions to the error $\Delta B_z/B_z$: 0.10 % from temperature drift effects, 0.03 % from the minor field components, 0.10 % from angular misalignment, and 0.05 % from the error on the z-position. Adding these errors linearly yields a total uncertainty of $\Delta B_z/B_z = 0.31\,\%$. Adding them in quadrature we obtain $\Delta B_z/B_z = 0.17\,\%$. In view of the accuracy requirement of $\Delta B_z/B_z \leq 0.40\,\%$, this is quite acceptable.

4. System Design

The design of the field measurement system follows the modularity of the muon detector which is subdivided into 16 independent "octants", 8 on each side of the central $z = 0$ plane (fig. 2). Each octant is equipped with 62 field sensors (see fig. 10).

On the outer chambers, two identical longitudinal strings of 13 field sensors have been installed: each time one in the middle and one near the edge. The probe positions along the strings were based on the 2-D model calculations, probes being placed at $\Delta B_z = 4 \cdot 10^{-3}$ T intervals. Two transverse strings of 6 probes each have been added near the high-z end of the outer chamber. The middle and inner chambers have each been equipped with two longitudinal strings only. Again probes have been placed every $\Delta B_z = 4 \cdot 10^{-3}$ T interval, yielding 4 and 6 probes per string for the middle and inner layers respectively. To cover the poles of the surface surrounding the magnetic volume, a string of 4 sensors has been affixed in the middle of the vertical end-frame of each octant. Irrespective of their locations, all sensors are oriented to measure the main component of the magnetic field (B_z). The entire field measuring system contains 992 field sensors.

4.1 Electronics

Fig. 11 gives a schematic overview of the read-out electronics of the system. It basically consists of an ADC and multiplexing electronics to select individual magnetoresistors for readout.

The resistances of the temperature compensated magnetoresistors are determined by measuring the voltage across the magnetoresistor for a constant electrical current. By chaining a number of probes in series, the same current flows through all probes in the chain. The read-out of the probes is accomplished through independent sense wires. An 8-channel differential analog multiplexer selects the signals from the individual channels. Eight of these multiplexers are combined on one card (PC-board) and have their outputs connected together. Only one multiplexer at a time is enabled. The differential output signal of the multiplexers is buffered through voltage followers and amplified. Via an analog switch the signal can be connected to a differential analog bus which is input to a 12-bits ADC. The design is virtually insensitive to the different DC levels at which the various probes in one chain operate. This is the result of the fully differential treatment of the signals up to the ADC and of the use of voltage followers ensuring a high input impedance and preventing parasitic currents through the sense wires which would disturb the measurement. Note that the fully differential design also provides a very good common-mode rejection.

The 8-channel multiplexer fixes the number of read-out positions in a single chain. For calibration purposes each chain has been equipped with a zero resistance position ($R_{\mathrm{short}} = 0\,\Omega$) measuring the offset and a field independent reference resistor R_{ref} which fixes the scale. The value of R_{sensor} is then determined from the raw ADC

values A_{sensor}, A_{short}, and A_{ref} as follows

$$R_{\text{sensor}} = \left\{ \frac{A_{\text{sensor}} - A_{\text{short}}}{A_{\text{ref}} - A_{\text{short}}} \right\} R_{\text{ref}}.$$

This method ensures that as long as the system has a linear response, it is intrinsically calibrated. Therefore neither the current source nor the amplification of the system are very critical with regard to medium and/or long term stability. A maximum of six read-out positions in each chain are available for field sensors. The 62 probes of one octant have been grouped into 13 "multiplexer chains". Unused channels are "filled" with dummy resistors.

The read-out system is controlled by a microprocessor. In order to read a particular sensor, the microprocessor operates the appropriate analog switch to select a card, it enables a multiplexer, and it addresses the proper multiplexer channel. A dummy A/D conversion allows the various signal levels to settle. The actual measurement involves four A/D conversions with 10 ms intervals to cancel the effects of possible 50 Hz pickup. The four ADC values are averaged and stored in memory. The entire procedure takes 50 ms per channel. The microprocessor continuously cycles through all channels to keep its memory up to date. It also communicates with the higher levels in the L3 monitoring subsystem and delivers the most recently measured resistance values when asked for. The microprocessor module is designed as a master in a VME-type crate which may contain up to 16 multiplexer cards. In the L3 experiment two crates are employed, one at each end of the detector. Each crate has its own processor and ADC module and serves 8 octants through 13 multiplexer cards. The distance between the crates and the probes is of the order of 40 m.

4.2 Mechanics

The probes have been mounted into hollow, rectangular aluminium bars, 3 cm wide and 1 cm high, with a slide-cover allowing access to its interior. Inside the bars are cubical precision supports on which the magnetoresistors are glued (see fig. 12). The supports are fastened by means of nylon fixation screws. The bars have been glued onto the outer surface of the muon drift chambers.

Basically, one bar contains all probes of one current chain. A multiwire screened cable connects to the multiplexer. Chains which extend over more than 1 m, have been subdivided into a couple of shorter bar-pieces which are interconnected via screened cable. To allow for a sufficiently accurate angular alignment, the minimum length of such a bar-piece is 25 cm. Electrical connections inside the bars are realised on PC-boards, which also carry the temperature compensation resistors.

4.3 Calibration

The calibration of the field probes consists of the following steps. First, the temperature characteristics of each individual probe are determined in order to fix

the value of the compensation resistor. Then the bars are assembled and placed in a homogeneous magnetic field for calibration. The bars which are a part of longitudinal strings are calibrated in a solenoidal magnet whereas a dipole magnet is used to calibrate the tranversely oriented bars. In both cases, the calibration field is monitored by means of an NMR probe. Prior to the actual calibration, the angular alignment of each probe is verified by rotating its support around the fixation screw to obtain maximum resistance reading. Note that the effect of a possible residual misalignment is largely calibrated out.

The probes are then calibrated by measuring their resistances in the absence of a field and for 8 magnetic field strengths in the range 0.36 to 0.60 T. During the calibration, the probes are read out with the same electronics as described above. For each probe, calibration constants have been determined by fitting the calibration data with a third order polynomial.

5. Field Reconstruction

For the L3 data analysis the values of the main and minor components are needed at any point (x, y, z) inside the fiducial volume of the detector. Since the eight-fold symmetry of the large magnet results to a good approximation in rotational symmetry, B_φ is neglible inside the fiducial volume. Therefore, we need only provide a map of B_z and B_r. The field map is obtained from a fit to the measured distribution of B_z-values. Two approaches are investigated to obtain a field map.

In a first approach, full cylindrical symmetry is assumed. All measured B_z-values from the magnetoresistors are projected onto one r-$z-$plane. Then a fit with a truncated Bessel function and a zero-order modified Bessel function is done to the data (there were in total 14 fit parameters). When using field measurements of the magnetoresistors in the longitudinal and transverse strings only (cf. chapter 4), the central region up to z-values of ± 4 m is well represented by this model. Nearly the full region can be well described if additional measurements near the magnet pole are used as input for the fit. These measurements can either be the sensors in the middle of the vertical endframe of each octant (cf. chapter 4) or the original calibration measurements taken on the inner surface of one of the magnet poles (cf. chapter 1). Only a small region at the extreme z- and r-corner does not meet the required precision. Here fit residuals of up to $5 \cdot 10^{-3}$ T are observed.

Since some 3-D effects are anticipated, a second approach is tried to achieve the required precision in the corners of the fiducial volume as well. In two slightly different models, an analytic representation of the fields of several octagonal, coaxial coils is used in conjunction with an approximate theoretical field map. The parameters defining these coils are adjusted in a fit to the measured B_z-values. This time, the 3-D spatial positions of the probes are used.

In the first model of this octagonal approach the approximate field map consists simply of a constant value. The currents of 17 "virtual", octagonal coils - located at the poles of the magnet - are adjusted in a fit to the measured B_z-values coming from two sets of measurements:
1. B_z-values from the magnetoresistors mounted on the muon chambers.
2. B_z-values from a priori field measurements.
The a priori measurements were performed before the installation of the physics detectors inside the magnet volume. They consist of measurements along the central axis with a mobile NMR probe, measurements from the region of one octant close to the pole piece and measurements from a plane perpendicular to the symmetry axis, inside the support tube at the limit of the magnet volume. The latter measurements were done with a mechanical gear with calibrated Hall plates which was also used to map the other three LEP experiments [7].

At this point it is important to note that, both here and in the 2-D case, especially the addition of measurement points near the boundary of the volume help to improve the results. An explanation of such an effect has already been given in [8].

In the second model, the approximate field map is calculated with the 2-D program POISSON. To this the fields of four "virtual" octagonal coils are added. Fit parameters are this time a common scale factor and a common displacement of the z-coordinate of the 2-D field map as well as three parameters for each of the four virtual coils, i.e. 14 parameters in total. Since the POISSON model already describes the field quite well and the virtual coils merely model the field deformations introduced by the inhomogeneities of the pole, only the B_z-values from the magnetoresistor measurements are used in this case to produce a field map.

Both octagonal models yield equivalent field maps which meet the accuracy requirements over the entire fiducial volume. Typical fit residuals of $\leq 2 \cdot 10^{-3}\,\mathrm{T}$ are obtained. Slightly worse residuals are encountered for the bottom octants in the high-z and high-r corners. This has been traced to the existence of large openings in the iron pole pieces of the magnet which accomodate the magnet door support rail and bearings. As these do not obey octagonal symmetry, they obviously cannot be described by the octagonal models.

The resulting B_z- and B_r-values as a function of z and r and for a φ-value of 11.25^o are shown in figs. 13 and 14 respectively (the shaded region in the r-$z-$plane contains no active detector components and is not part of the fiducial volume). The main field component is rather homogeneous for $z = 0$, increasing from 0.500 T in the centre ($r = 0$) to 0.525 T at $r = 5.5\,\mathrm{m}$. Along the beam axis B_z drops because the pole piece has a large hole in the center. Close to the inner opening of the pole piece an inhomogeneous region is characterized by an increase of B_z and B_r. In the center B_r is very small increasing only to 0.06 T in the region of the outer muon chambers close to the pole. The results are in very good agreement with the 2-D calculations described in chapter 2. The field map obtained through the procedure described here is being applied in the L3 analysis software on a routine basis.

6. Results and Conclusions

In its first years of operation, the field measuring system proved to be very reliable. On initial turn-on, three out of the total 992 installed field probes gave no proper signal, probably due to shorts and/or broken wires. However, as the system has a substantial amount of redundancy, this poses no serious problem. No other dead channels have developed since.

The magnetoresistors and the five permanently installed NMR probes are read out on a bimonthly basis since the middle of 1989 as a new fieldmap has to be produced as soon as a significant change is observed. The L3 magnetic field turns out to be very stable. No changes larger than 0.3 % have been observed up to now. We find the magnetoresistor readings to scale within 0.1 % with the independent readings of the NMR probes.

In conclusion, we successfully developed and implemented a magnetic field measuring system for a very large magnet volume, giving an accuracy of better than 0.4 %. We demonstrated that low cost devices (magnetoresistors) can be used as precision sensors in such a system. When thinking of possible other applications one should however keep its limitations in mind. It works for one magnetic field component only and other components should be relatively small. Moreover, the calibration of the sensors is a rather laborious procedure, and the resulting calibration only yields the required precision over a limited range of field values and ambient temperatures.

Acknowledgements

We would like to thank H. Wind for useful discussions. We thank D. Lehm and G. Stefanini for their help with the a priori measurements and we thank the ALEPH collaboration for the use of its test solenoid.

References

[1] B. Adeva et al., Nucl. Instr. and Meth. A289 (1990) 35.
[2] J. Onvlee, "The Behaviour of the L3 Muon Chambers in a Magnetic Field", Ph.D. Thesis, University of Amsterdam, (1989), unpublished.
[3] D.J. Schotanus, Nijmegen Report HEN-283, (1987), unpublished.
[4] R. Holsinger, C. Iselin, CERN program library T604, unpublished.
[5] J. Simkin, C.W. Trowbridge, IEE Proc. B127 (1980) 368.
[6] Siemens Datenbuch 1982/83, Sensoren Teil 1, Magnetfeldhalbleiter.
[7] L. Bauerdick, G. Petrucci, G. Stefanini, ALEPH 88-034, (1988), unpublished.
[8] H. Wind, IEEE Trans. Magn. 5 (1969) 269.

Figure Captions

Fig. 1. General view of the L3 detector. Moving toward the interaction point: magnet yoke, magnet coil, muon drift chambers, hadron calorimeter, BGO electromagnetic calorimeter, and time expansion chamber.

Fig. 2. View of the muon spectrometer, subdivided into 16 independent "octants".

Fig. 3. Schematic view of muon track measurement in one octant. Coming from the interaction point (I.P.), the muon traverses three layers of drift chambers. From the hits in each of the layers, the sagitta s is evaluated.

Fig. 4. Main field component B_z at the octant outer surface as calculated with the 2-D program POISSON. The curve for $r = 5.6\,\mathrm{m}$ corresponds to the centre of the octant surface, the $r = 6.0\,\mathrm{m}$ curve corresponds to the edge of the octant.

Fig. 5. Simplified view of current path through magnetoresistor in the absence of a magnetic field ($B = 0$) and for a magnetic field normal to the plane of the probe ($B \neq 0$).

Fig. 6. Magnetoresistance R_B in function of the applied magnetic field B as measured for three different magnetoresistors.

Fig. 7. Temperature behaviour of magnetoresistance
a) bare magnetoresistor ($B = 0.5\,\mathrm{T}$)
b) compensated magnetoresistor ($B = 0.5\,\mathrm{T}$)
c) compensated magnetoresistor ($B = 0.4\,\mathrm{T}$)
Note the expanded vertical scale in figures b) and c).

Fig. 8. Schematic drawing of FP30N60 K magnetoresistor defining the rotation axes I and II (see text). The shaded loop indicates the pattern of active material.

Fig. 9. Decomposition of radial field component B_r into "horizontal" and "vertical" components B_h and B_v.

Fig. 10. Projective view of muon chamber octant with dots indicating the locations of the magnetic field sensors. Note that the sensors in the central rows on the inner and middle layers of drift chambers (see text) are not visible in this projection.

Fig. 11. Schematic overview of magnetoresistor read-out electronics.

Fig. 12. Magnetoresistor support and mounting structure.

Fig. 13. The main field component B_z as a function of r and z ($\varphi = 11.25^o$). The shaded region in the r-z−plane is not part of the fiducial volume of the detector.

Fig. 14. The radial field component B_r as a function of r and z ($\varphi = 11.25^o$). The shaded region in the r-z−plane is not part of the fiducial volume of the detector.

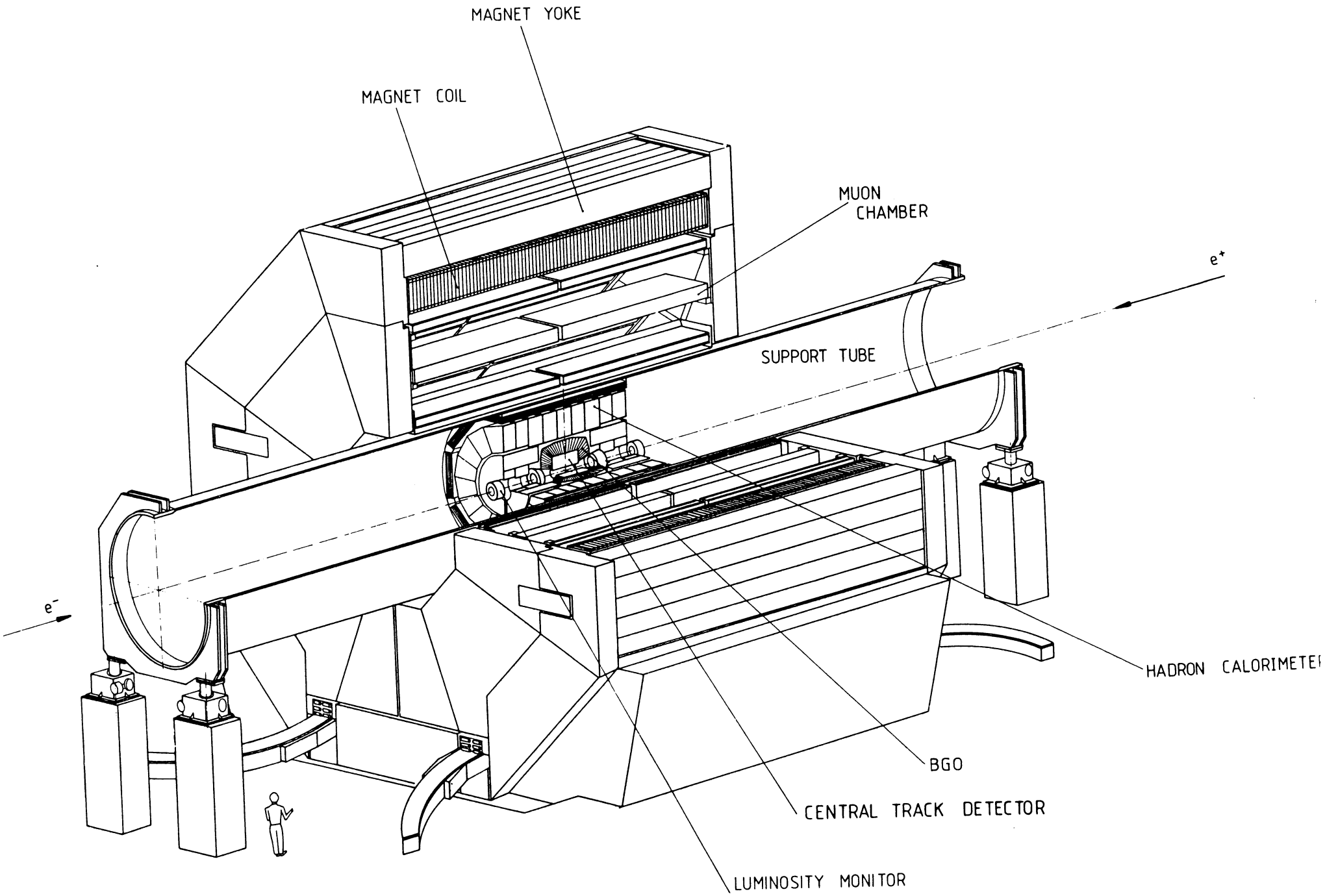
MAGNET YOKE
MAGNET COIL
MUON
CHAMBER
e+
SUPPORT TUBE
e-
HADRON CALORIMETER
BGO
CENTRAL TRACK DETECTOR
LUMINOSITY MONITOR

Figure 1.

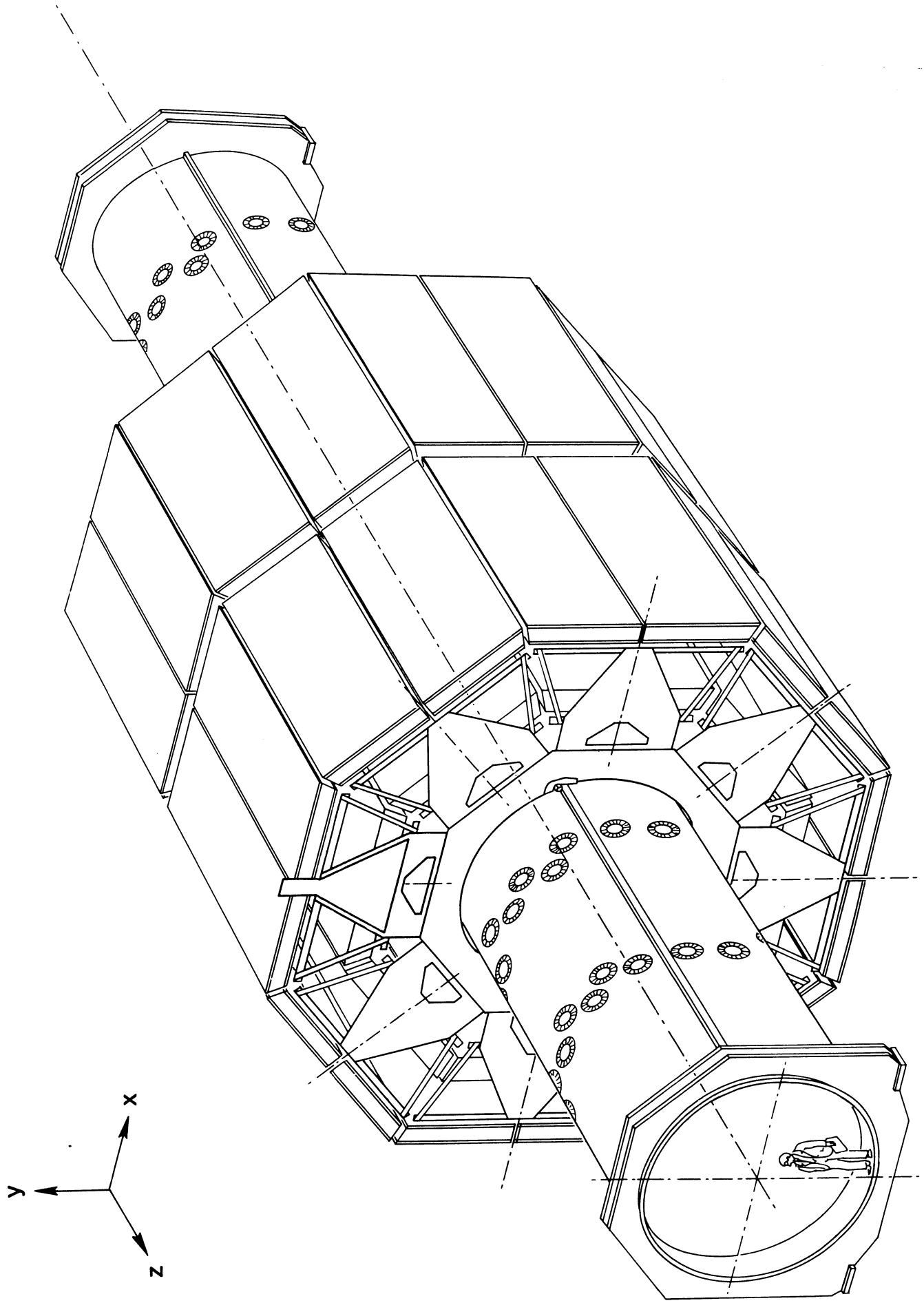

Figure 2.

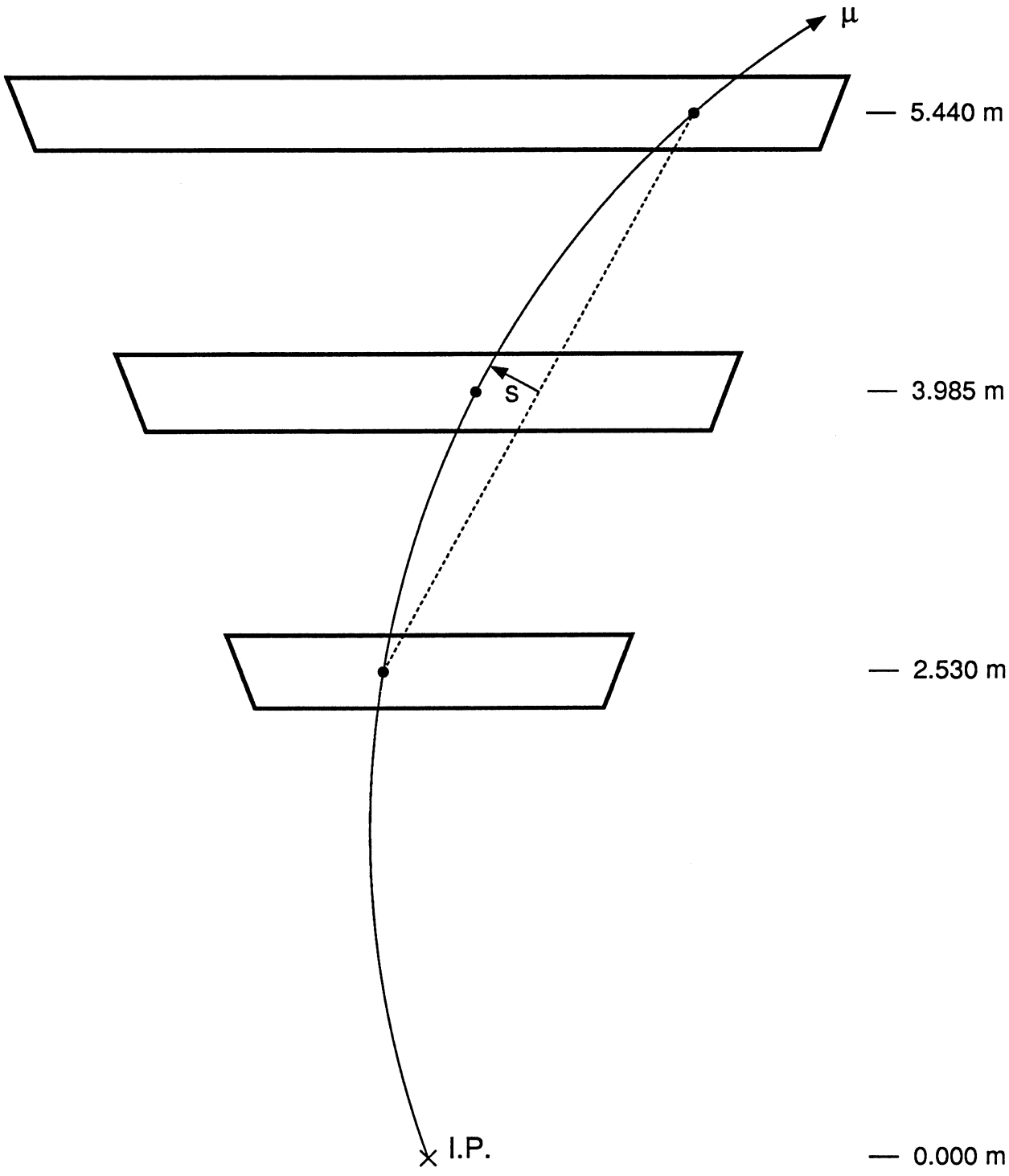

Figure 3.

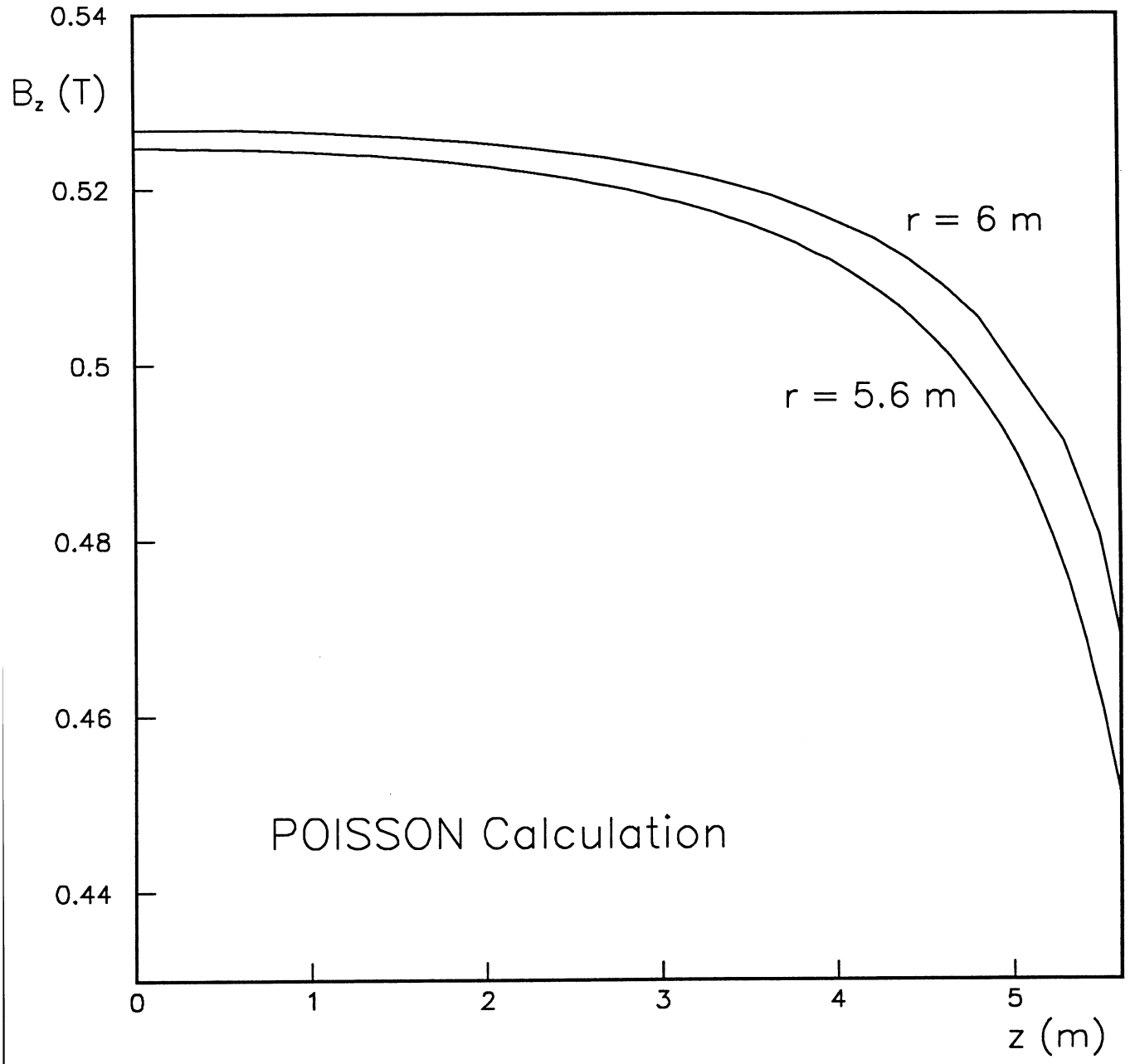
0.54
B_z (T)
0.52
0.5
0.48
0.46
0.44
r = 6 m
r = 5.6 m
POISSON Calculation
0
1
2
3
4
5
z (m)

Figure 4.

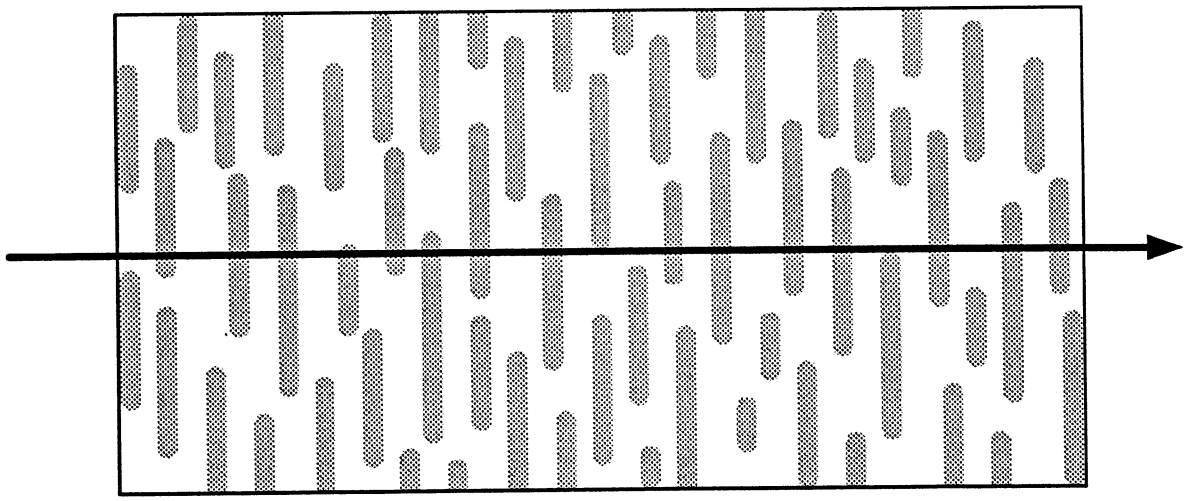

B=0

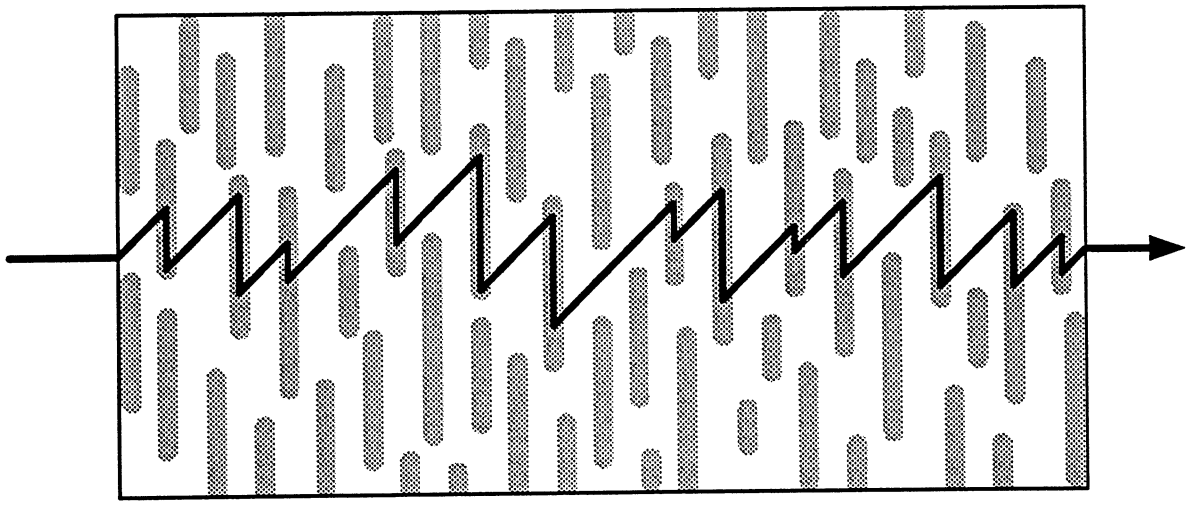

B≠0

Figure 5.

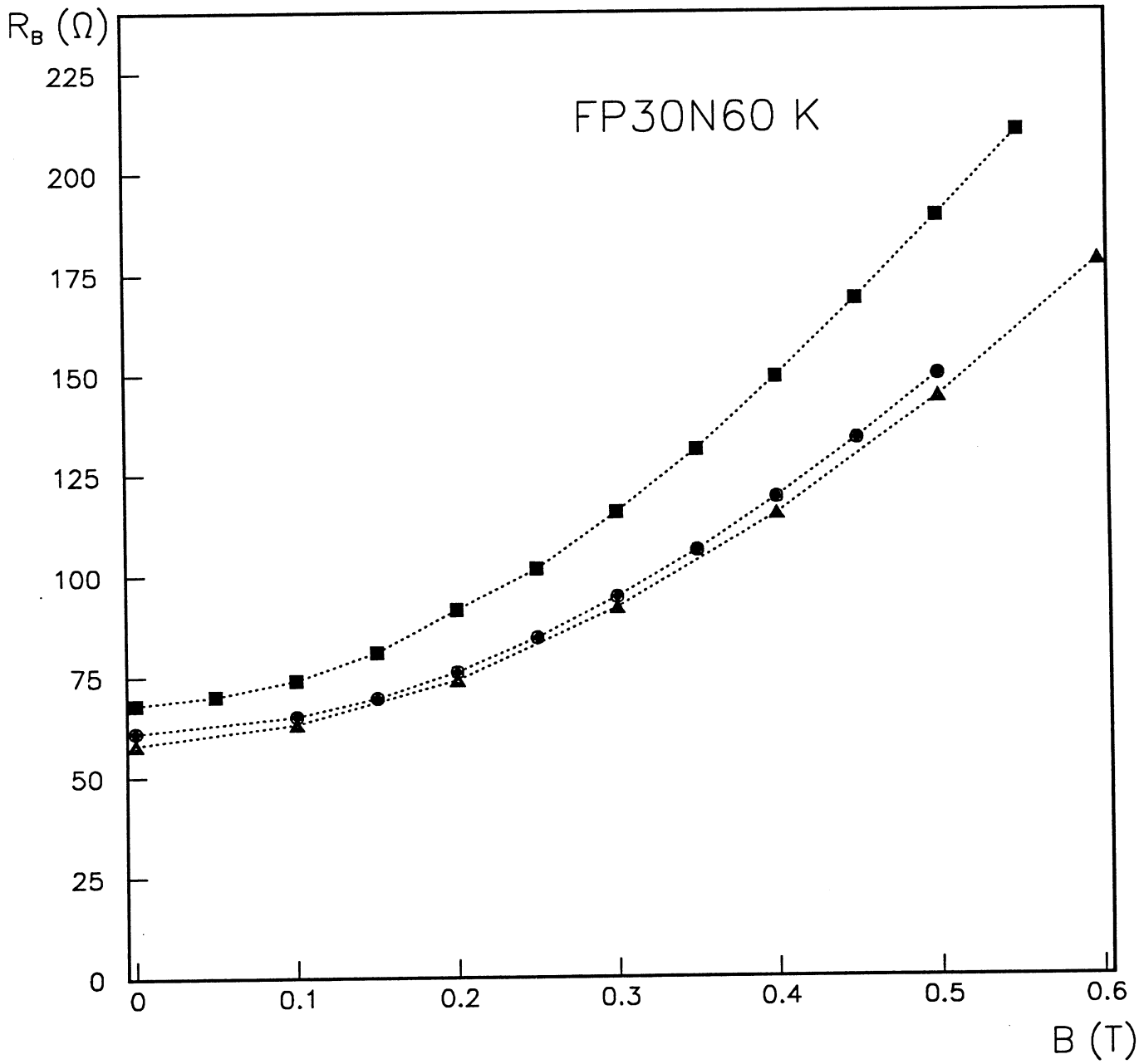
R_B (Ω)
225
200
175
150
125
100
75
50
25
0
FP30N60 K
0
0.1
0.2
0.3
0.4
0.5
0.6
B (T)

Figure 6.

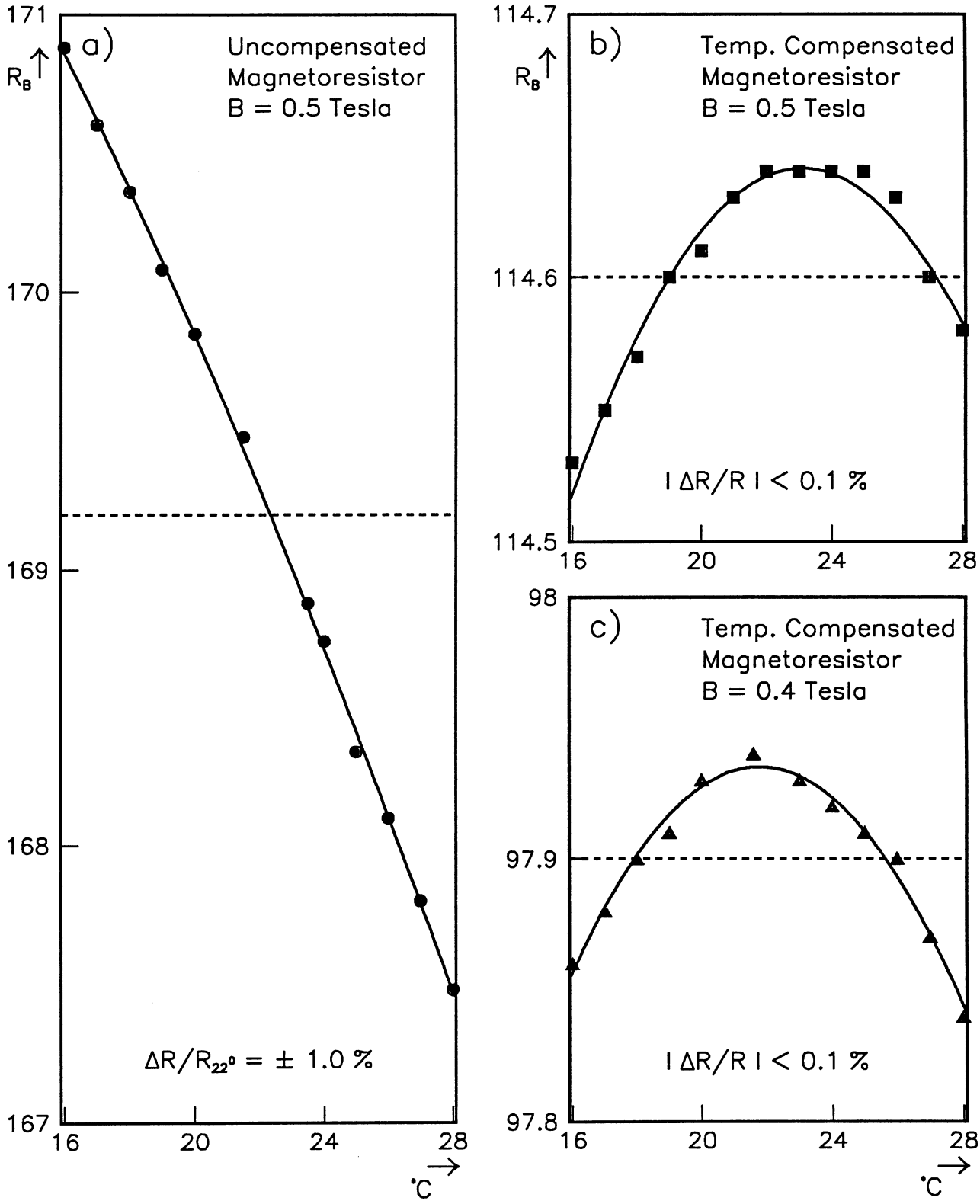
171
R_B
a)
Uncompensated
Magnetoresistor
B = 0.5 Tesla
170
169
168
167
$\Delta R/R_{22^\circ} = \pm$ 1.0 %
16
20
24
28
°C
114.7
R_B
b)
Temp. Compensated
Magnetoresistor
B = 0.5 Tesla
114.6
114.5
| ΔR/R | < 0.1 %
16
20
24
28
98
c)
Temp. Compensated
Magnetoresistor
B = 0.4 Tesla
97.9
97.8
| ΔR/R | < 0.1 %
16
20
24
28
°C

Figure 7.

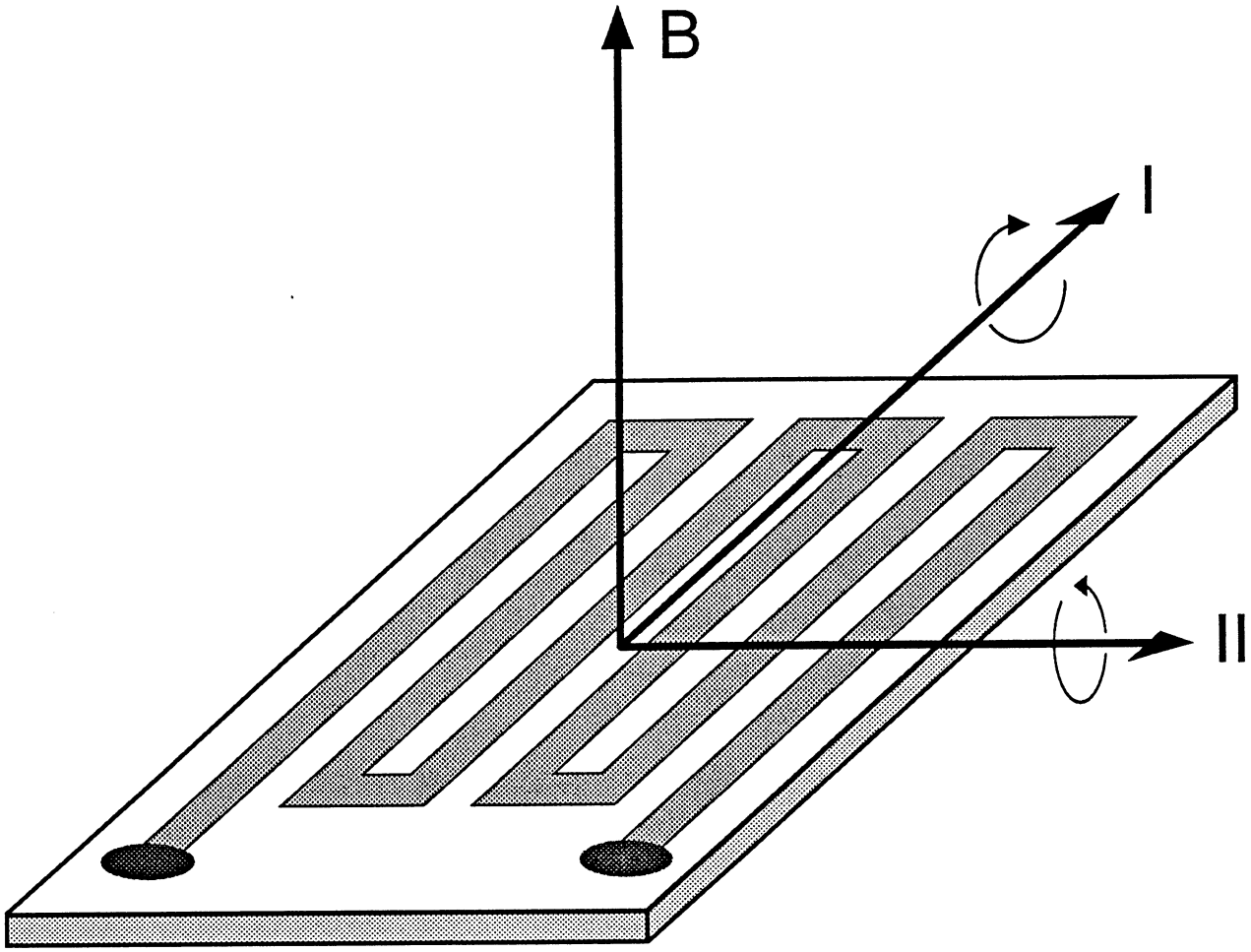

Figure 8.

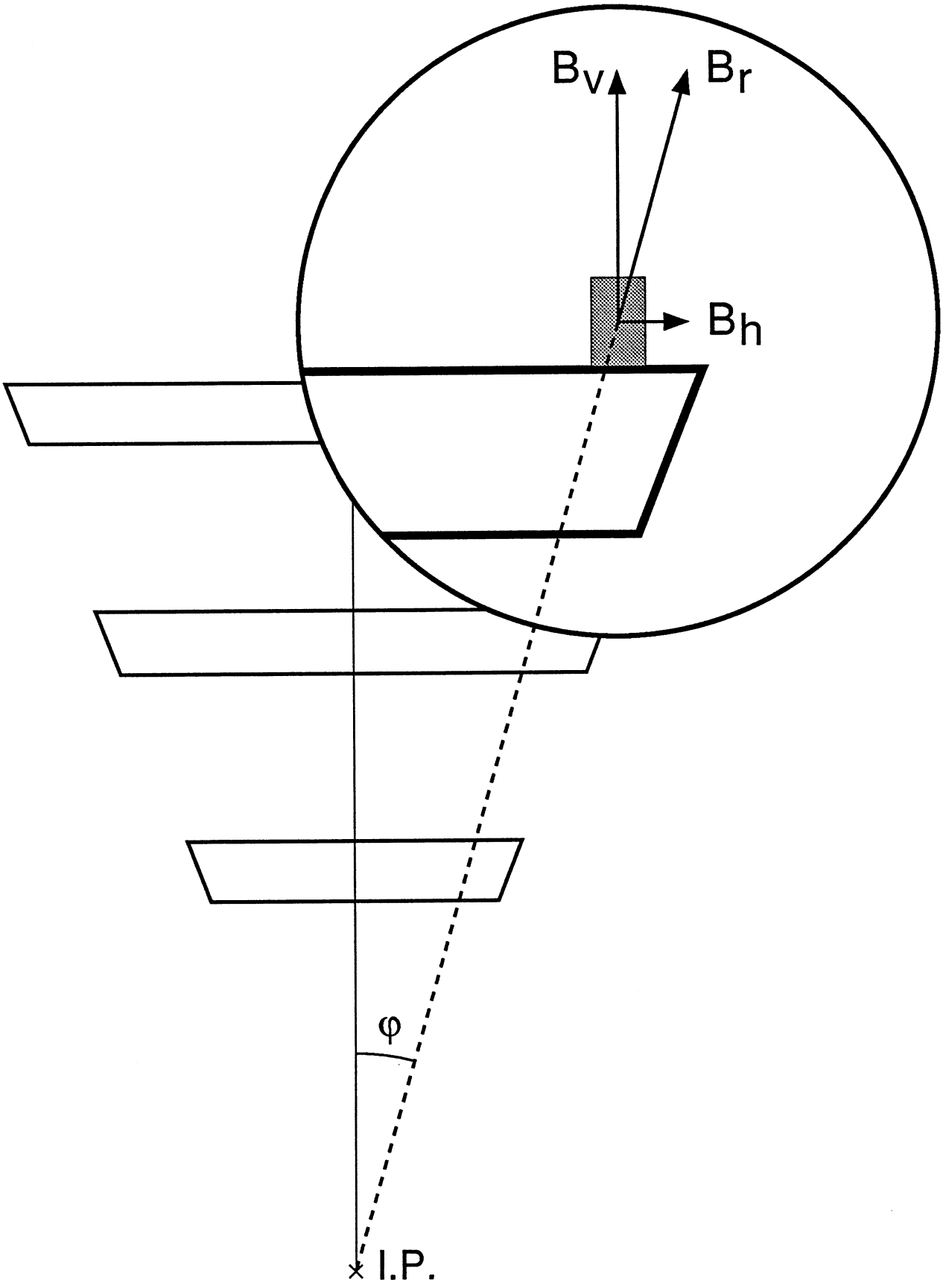

Figure 9.

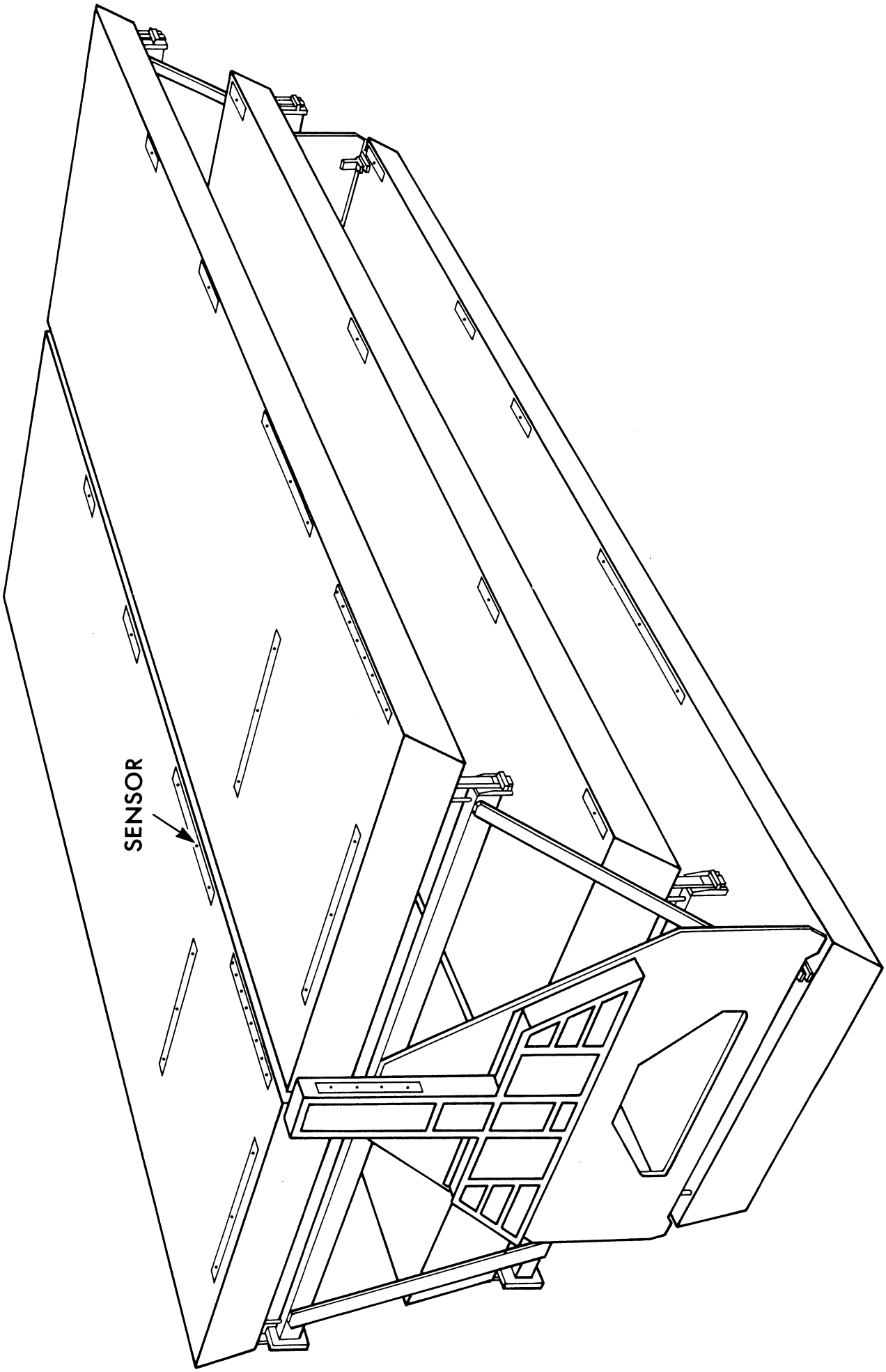

Figure 10.

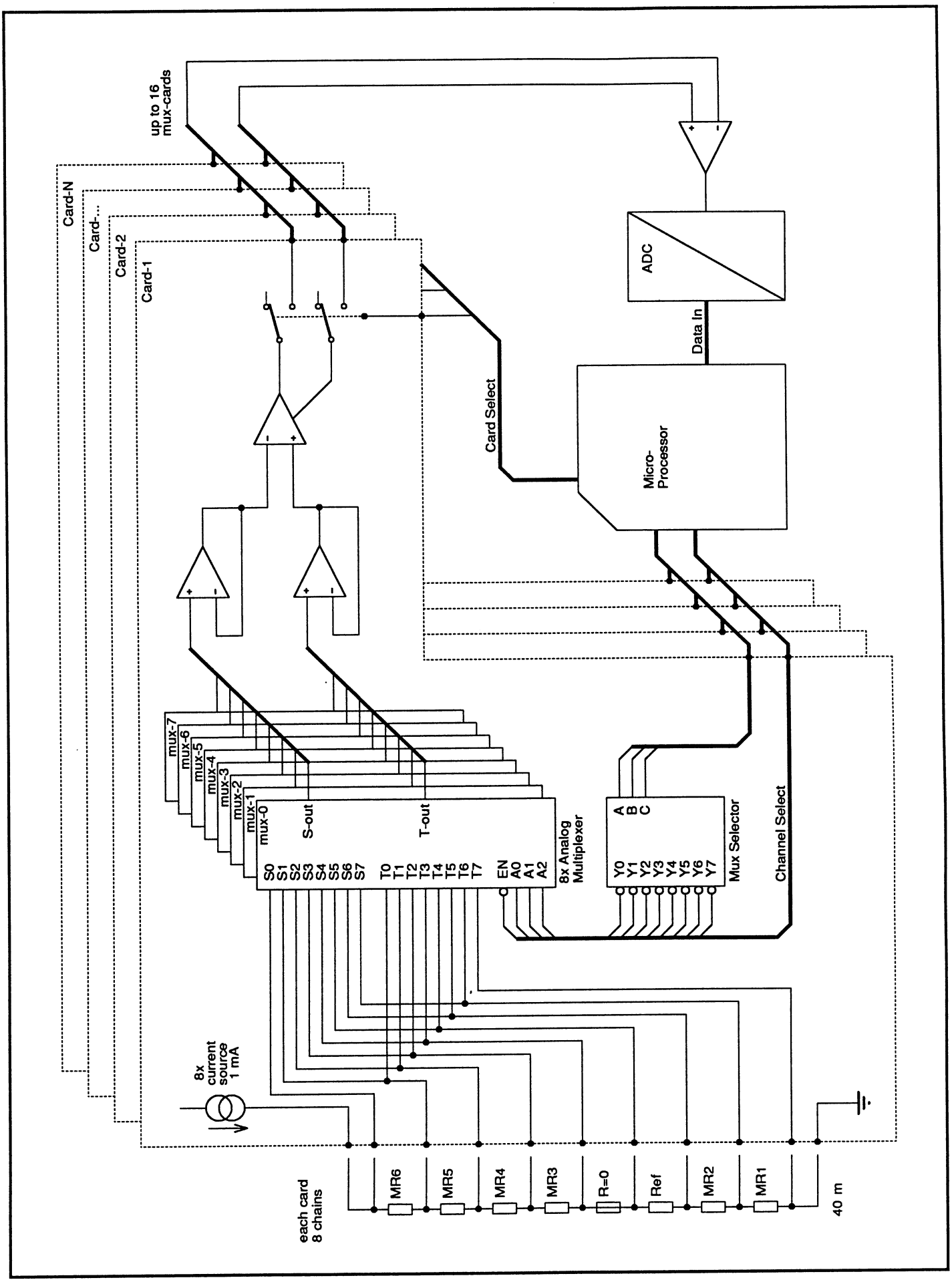
up to 16
mux-cards
Card-N
Card-...
Card-2
Card-1
ADC
Data In
Card Select
Micro-
Processor
mux-7
mux-6
mux-5
mux-4
mux-3
mux-2
mux-1
mux-0
S-out
T-out
S0
S1
S2
S3
S4
S5
S6
S7
T0
T1
T2
T3
T4
T5
T6
T7
EN
A0
A1
A2
8x Analog
Multiplexer
A
B
C
Y0
Y1
Y2
Y3
Y4
Y5
Y6
Y7
Mux Selector
Channel Select
8x
current
source
1 mA
each card
8 chains
MR6
MR5
MR4
MR3
R=0
Ref
MR2
MR1
40 m

Figure 11.

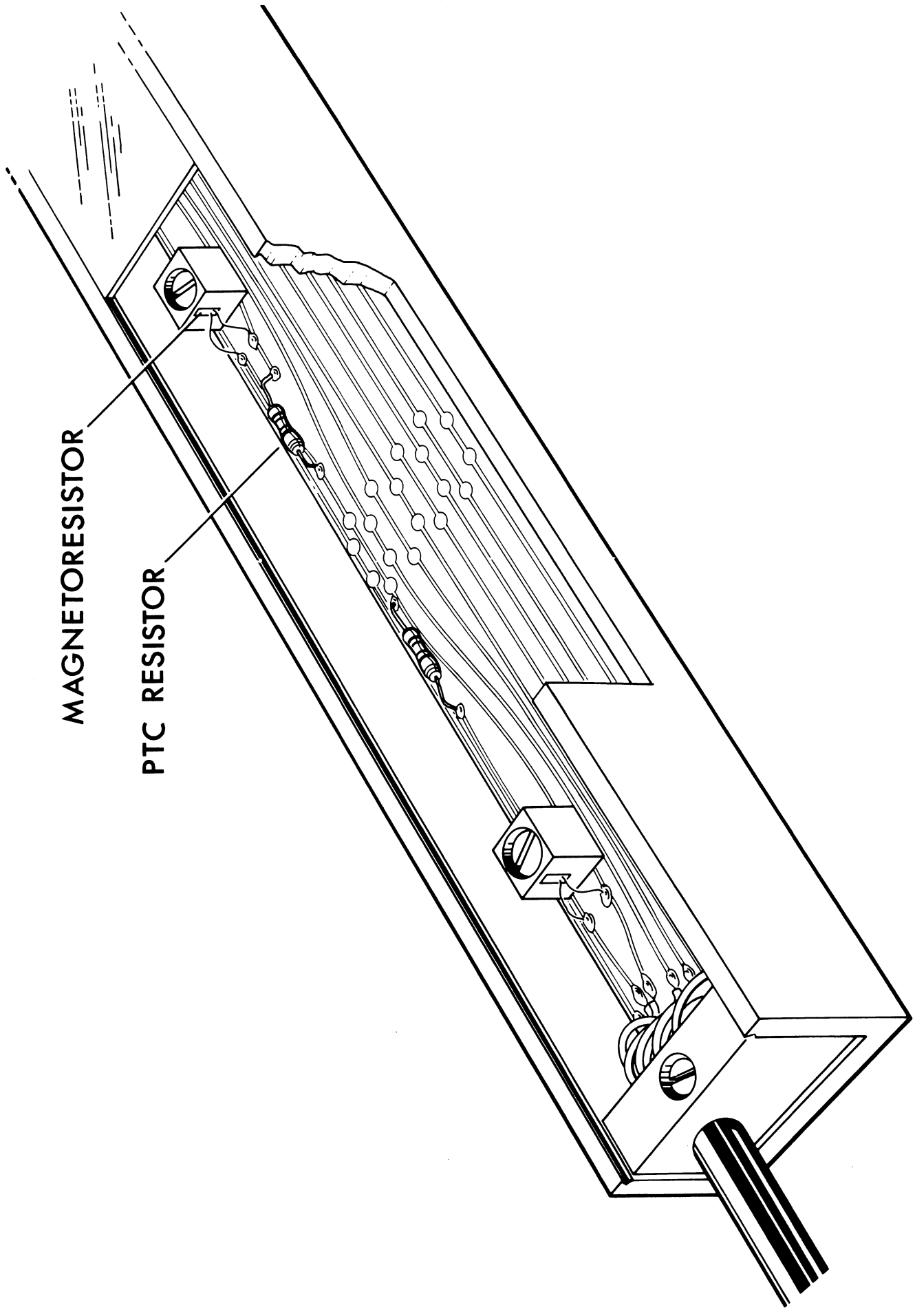

Figure 12.

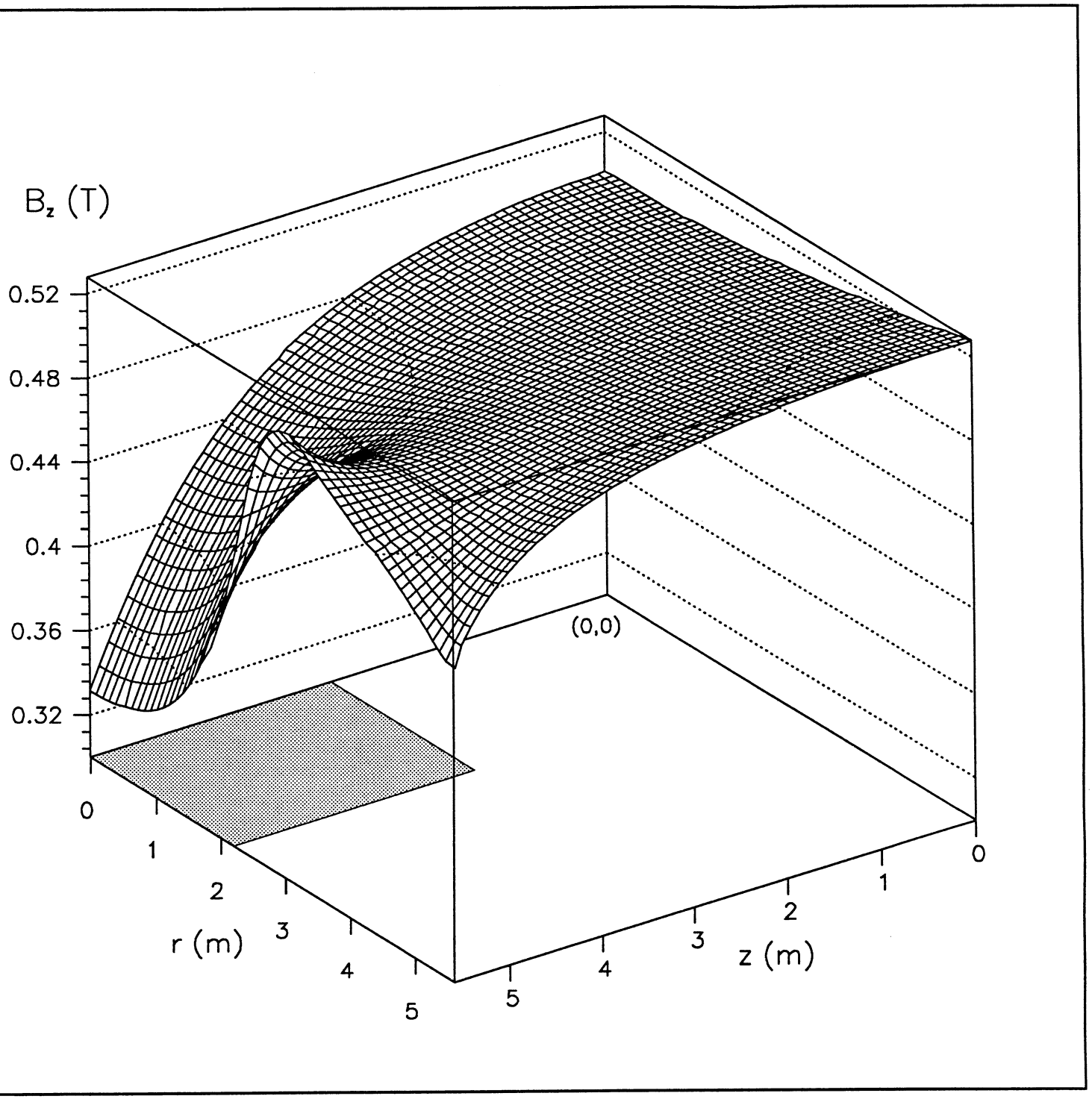

Figure 13.

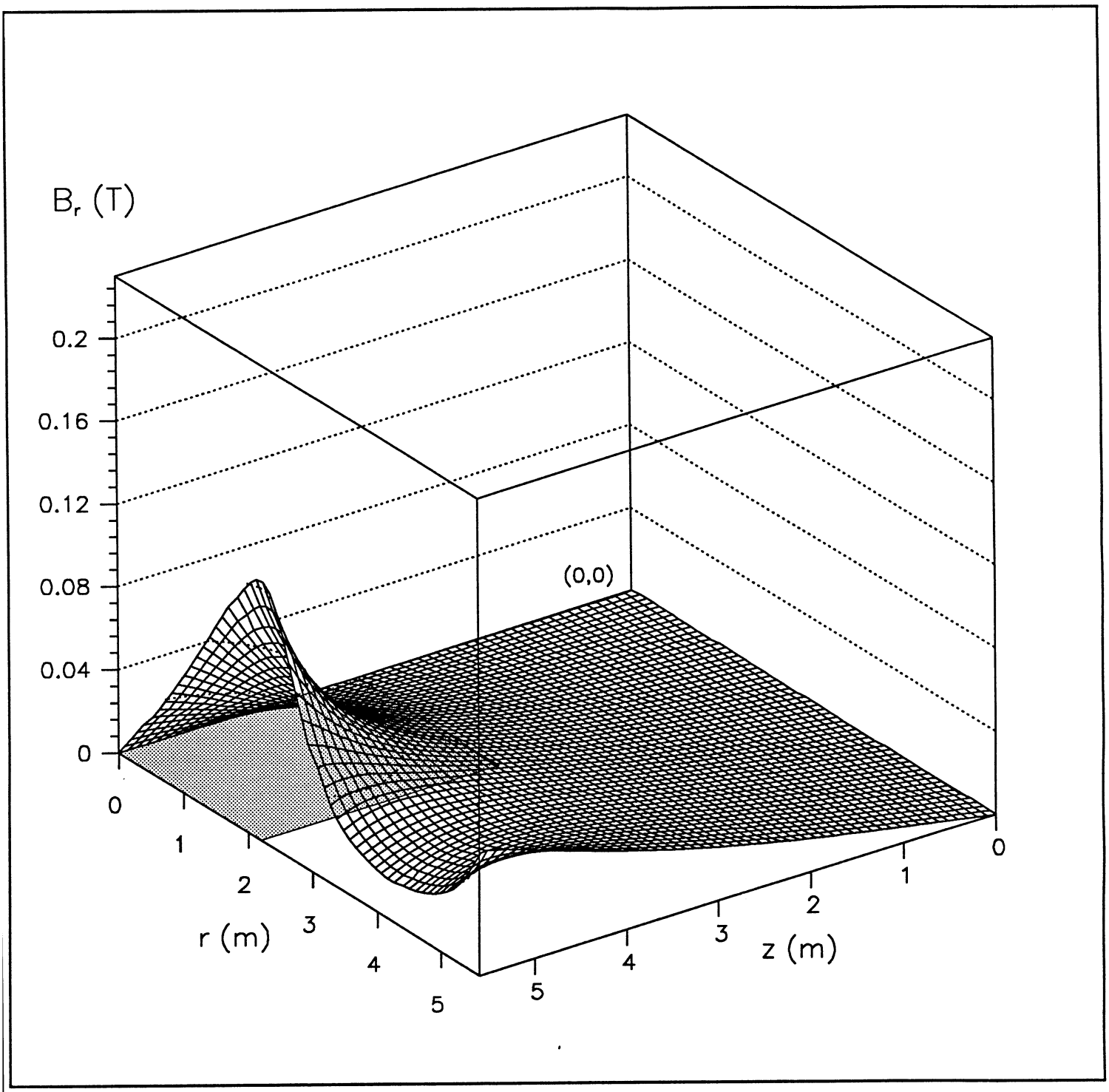

Figure 14.